Appl Biochem Biotechnol
DOI 10.1007/s12010-015-1887-5

Low-Cost Synthesis of Smart Biocompatible Graphene Oxide Reduced Species by Means of GFP

Tiziana Masullo[1] · **Nerina Armata**[2] · **Flavio Pendolino**[3] · **Paolo Colombo**[4] · **Fabrizio Lo Celso**[2] · **Salvatore Mazzola**[5] · **Angela Cuttitta**[1]

Received: 8 May 2015 / Accepted: 4 October 2015

Abstract The aim of this work is focused on the engineering of biocompatible complex systems composed of an inorganic and bio part. Graphene oxide (GO) and/or graphite oxide (GtO) were taken into account as potential substrates to the linkage of the protein such as *Anemonia sulcata* recombinant green fluorescent protein (rAsGFP). The complex system is obtained through a reduction process between GO/GtO and rAsGFP archiving an environmentally friendly biosynthesis. Spectroscopic measurements support the formation of reduced species. In particular, photoluminescence shows a change in the activity of the protein when a bond is formed, highlighted by a loss of the maximum emission signal of rAsGFP and a redshift of the maximum absorption peak of the GO/GtO species. Moreover, the hemolysis assay reveals a lower value in the presence of less oxidized graphene species providing evidence for a biocompatible material. This singular aspect can be approached as a promising method for circulating pharmaceutical preparations via intravenous administration in the field of drug delivery.

Keywords Graphene oxide · Graphite oxide · GFP · Reduction · Biocompatibility · Hemolysis

Tiziana Masullo, Nerina Armata and Flavio Pendolino contributed equally to this work.

✉ Angela Cuttitta
angela.cuttitta@iamc.cnr.it

[1] National Research Council, Institute for Coastal Marine Environment, UOS Capo Granitola, Laboratory of Molecular Ecology and Biotechnology, Torretta Granitola, 91021 Trapani, Italy

[2] Department of Physics and Chemistry, Viale delle Scienze Ed17, 90128 Palermo, Italy

[3] Department of Physics and Astronomy "Galileo Galilei", University of Padova, Via Marzolo 8, 35131 Padova, Italy

[4] National Research Council, Institute of Biomedicine and Molecular Immunology (IBIM), Via Ugo La Malfa, 153, 90146 Palermo, Italy

[5] National Research Council, Institute for Coastal Marine Environment, Calata Porta di Massa, 80133 Naples, Italy

Published online: 21 October 2015

Introduction

The recent interest in graphene oxide (GO) and reduced graphene oxide (rGO) is growing, aimed at finding a more worthy and scalable method for producing pristine graphene. In the last decade, a number of different approaches have been developed for the preparation of pristine graphene including the mechanical exfoliation of graphite [1], chemical exfoliation of graphite [2], unzipping of carbon nanotubes [3], and epitaxial growth on silicon carbide (SiC) surfaces [4]. However, the solution-based chemical synthesis is considered one of the most efficient approaches for low-cost and large-scale production. In this context, GO and rGO were considered materials with distinct properties. Because a change in the pristine graphene structure opens a gap at the Fermi level [5], the selective reduction of GO allows for a modulation of rGO properties, bringing the possibility of employing either GO and rGO in several technological fields for applications such as conductive films [6], hydrogen production and energy storage [7, 8], emulsifying organic solvents for industrial processes [9], and biosensors [10, 11]. For this reason, the methods used for the synthesis of graphene materials are important because those procedures imply chemical reactions that involve hazardous and toxic reagents. GO reduction was recently investigated and reported in a number of publications using thermal reduction [12, 13] or various reducing agents in an aqueous medium such as hydrazine and hydrazine derivatives [14–18], sodium borohydride [14, 19], or lithium aluminum hydride [19]. In addition, other methods were developed using different biomolecules, i.e., ascorbic acid [18, 20], enzymes [21], amino acids, glucose, and bovine serum albumin as reducing agents or stabilizers [7, 17, 22, 23]. The use of a recombinant enhanced green fluorescent protein (GB: U57607) has been proposed as a new protocol for the biocompatible reduction of the GO species [24]. Thanks to its biocompatibility and biological inertia [25, 26], the chemical structure of green fluorescent protein (GFP) makes it a perfect reducing and real capping agent for graphene and graphite oxides. Indeed, in the enhanced green fluorescent protein (EGFP), as in the rAsGFP, the thiol group of the five residues of cysteine can be oxidized to form the disulfide derivative cysteine, which acts as a nucleophile [27]. In our work, we have tested the *Anemonia sulcata* recombinant green fluorescent protein (rAsGFP) as a reducent for graphene oxide (GO) and graphite oxide (GtO) species. rAsGFP is a protein of 228 amino acids with a putative MW of 24 kDa. It is stable in many solvents and has a theoretical pI of 6.45. The reduced GO and GtO species, aggregated to the rAsGFP, have been characterized by means of spectroscopic techniques. Moreover, the scientific community is focusing the attention on the biological applications of graphene sheets (GS) and graphene oxide (GO) for their great potential role in bacterial inhibition [28], drug delivery [29], and photothermal therapy [30]. The biocompatibility and toxicological activity of graphene-related materials using many cellular lines is the object of the study [29, 31–34]. Thus, since the materials studied in this work could find biomedical applications [28, 29, 31, 35–37], the cytotoxicity of GO, GtO, and the corresponding species bound to rAsGFP have been tested in human erythrocytes (RBCs), by means of the hemoglobin measurement consequent to the cell lysis. In fact, intravenous administration is the preferred mode of systemically introducing pharmaceutical preparation for imaging, drug delivery, or therapy. Moreover, GFPs are used as noninvasive probes to study various biological models. They are tools for different applications as follows: protein labeling, imagining of target-gene promoter up- and downregulation, detection of protein–protein interactions, tracking protein movement, and monitoring cellular parameters [38, 39].

Materials and Methods

The following chemicals were used as received: $KMnO_4$ (Sigma-Aldrich), H_2SO_4 (98 %, Sigma-Aldrich), HCl (37 %, Sigma-Aldrich), and expanded graphite ECOPHIT 50 grains (size 40–50 m). Commercial graphene oxide was purchased from Graphenea with a carbon/oxygen ratio of 1:1. The rAsGFP is a recombinant protein expressed in *Escherichia coli* and produced as a highly purified protein starting from a cDNA of 687 bp isolated from the total RNA of *A. sulcata* tentacles [40].

Synthesis of GO and GtO

The synthesis of graphene oxide was performed using a Modified Sun protocol, as described in our previous work [41]. In short, expanded graphite (2.5 g) and $KMnO_4$ (7.5 g) were mixed until homogeneity. Concentrated sulfuric acid (50 mL) were added slowly (exothermic reaction) with continuous stirring (magnetic stir bars) until a petrol-green liquid paste was obtained. A spontaneous volumetric expansion is obtained. Next, the hydrolysis process (200 mL of distilled water) is taken for 1 h at 90 °C. Finally, the product is washed in a paper filter with distilled water, HCl 0.15 M, and distilled water. The material is dried in an oven at 70 °C for 3 days. A similar approach is used for producing graphite oxide. In this latter synthesis, each reaction step is kept in an ice bath producing a black powder suppressing the volumetric expansion step.

Synthesis of rAsGFP-rGO and rAsGFP-rGtO

Samples (GO and GtO) (1 mg mL^{-1}, pH 7) were prepared by dispersing the solid in Milli-Q water and sonicating for 15 min at RT. The dispersions were stirred for 1 h at 300 rpm and centrifugated for 5 min at 10,000 rpm before analyzing the soluble fractions. Using GO and GtO as a precursor, our rAsGFP has been used as a reductant and stabilizer. A mixed aqueous solution (pH 7) containing rAsGFP (1 μM) and GO or GtO (1 mg mL^{-1}) was sonicated for 15 min, and the mixture was maintained at 40 °C for 1 h. The mixtures were then cooled to room temperature for a further 15 min. Subsequently, the mixtures were stirred at 90 °C for 1 h at 400 rpm. The resulting black dispersions were centrifuged and then washed with water. Finally, homogenous rAsGFP-rGO and rAsGFP-rGtO suspensions were obtained.

Spectroscopic Measurements

UV–Vis spectra were recorded in UV2700 spectrometer (Shimadzu) with a quartz cell. Fourier transform infrared spectroscopy (FTIR) measurements were carried out in a Jasco70 FT/IR-620 spectrometer using KBr pellets. Photoluminescence measurements were performed on a RF 5301PC spectrofluorometer (Shimadzu) using 5 nm spectral slit widths for excitation and emission.

In Vitro Hemolytic Activity

Two and a half milliliters of whole blood, from volunteer donors, was added to 10 mL of 1× Dulbecco's phosphate buffered saline (Ca^{2+}/Mg^{2+} free) and centrifuged at 500×*g* for 10 min to isolate RBCs from the serum. This purification step was repeated five times, and then the

washed RBCs were diluted to 25 mL in 1× PBS. To test the hemolytic activity of our samples, 0.2 mL of diluted RBC suspension (around 3.5×10^8 cells mL^{-1}) was added to 1 mL of each sample suspension solution at different concentrations (range from 3 to 200 μg mL^{-1}). Distilled water (+RBCs) and 1× PBS (+RBCs) were used as the positive and negative control, respectively. All the samples were placed on a rocking shaker in an incubator at 37 °C for 3 h, as suggested [42]. After incubation, the samples were centrifuged at 10,000×*g* for 3 min. The hemoglobin absorbance in the supernatant was measured at 450 nm using an iMark microplate reader (Bio-Rad). The percent hemolysis was calculated using Eq. 1:

$$\%\ \text{hemolysis} = \frac{\text{abs}_{\text{sample}} - \text{abs}_{\text{negative control}}}{\text{abs}_{\text{positive control}} - \text{abs}_{\text{negative control}}} \quad (1)$$

After 3 h of incubation at 37 °C, the suspensions of RBCs were observed under a LEICA ICC50 HD microscope (using a ×20 objective lens) in order to value the cell lysis.

Results and Discussion

The alternative production method used for graphene or graphite oxides has allowed us to obtain the pristine for single (GO) and multilayer (GtO) derivative oxide carbon materials with a low content of oxygen (around 20 %). Moreover, the further reduction of GtO and GO species conducted by means of rAsGFP seems to be a promising environmentally friendly procedure which not involves any organic solvent or harmful chemicals.

Spectroscopic Characterization

Spectroscopic investigation is used in our work to obtain information about the behavior of the graphene and graphite oxide species and relative reduced products. In particular, we studied the absorption and photoluminescent characteristics of each sample in water at pH 7 before and after the reaction with the rAsGFP. Information about the functional group (carbonyl, hydroxyl, epoxy) and/or linkages sites (C–S) were investigated by means of FTIR. UV–Vis spectra for GO and GtO water dispersion are investigated in the range 190–900 nm. In the region from 400 to 900 nm, we did not identify absorption bands (Fig. 1a, b). The maximum absorbance for GO takes place at about 230 nm with a shoulder at 300 nm (see Fig. 1a). The GO absorption peak at 230 nm is attributed to the conjugated systems, and the shoulder at 300 nm is due to the C=O transition. A change of the optical absorption is found in the GtO spectrum where the maximum absorbance is shifted to lower wavelengths (196 nm) and the shoulder at 300 nm almost entirely disappears (Fig. 1b). This fact was investigated by Lai et al. [43] combining results from the UV–Vis spectra and AFM technique to extract information about the number of layers. The authors claimed that for the monolayer, a corresponding UV–Vis spectrum is observed with a maximum absorbance at 230 nm and a shoulder around 300 nm, instead, when the number of non-exfoliated layers was increased, the shoulder disappears and maximum peak vanishes for thick layer greater than ten layers. Therefore, we can reasonably affirm that our GO is a monolayer dispersion and GtO is a multilayer dispersion due to their structure. Those two materials show diverse activity. In fact, the reduction of GO and GtO is confirmed by the UV–Vis spectra (Fig. 1a, b). A redshift of the maximum absorbance peak, from 236 to 247 nm, is observed for rAsGFP-rGO (see Fig. 1a). This effect is magnified in the

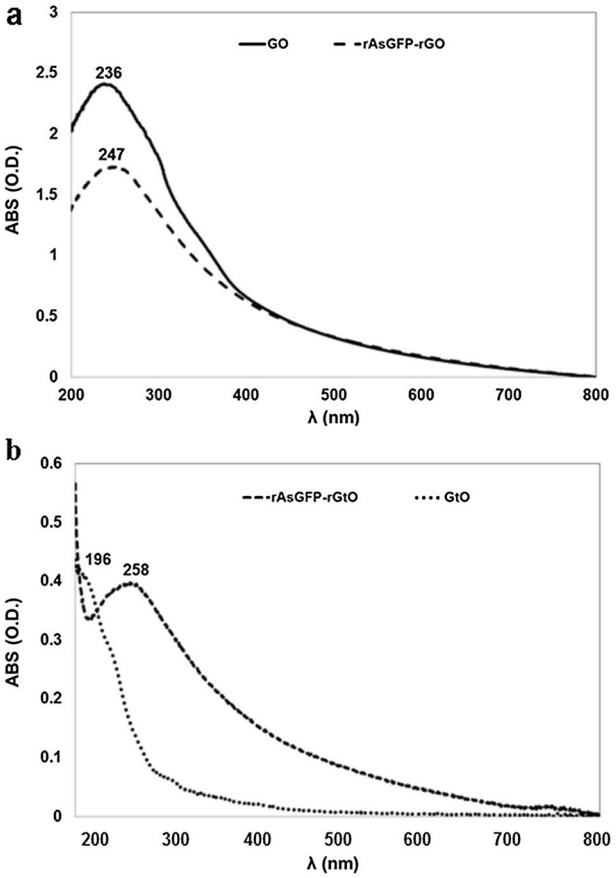

Fig. 1 UV–Vis spectra of the **a** GO (*solid line*) and rAsGFP-rGO (*dashed line*), and **b** GtO (*point line*) and rAsGFP-rGtO (*dashed square line*)

case of rAsGFP-rGtO with a shift to lower wavelengths of about 62 nm (see Fig. 1b). The redshift of the maximum absorbance peak may attribute to the increase of the atomic percentage of the sp^2 hybridized carbon atoms with an increase of reduction time [44]. The disappearance of the absorption shoulder at 300 nm after reduction suggests the removal of carbonyl functional groups [45]. Figure 2 shows FTIR spectra for the GO and GtO dispersions and their mixtures with rAsGFP. The GO spectrum (Fig. 2a) was described in detail in our previous work [46] and exhibits the following characteristic bands: 3440 cm^{-1} corresponds to the O–H stretching vibrations, tiny doublet peaks at 2920 and 2850 cm^{-1} correspond to the symmetric and antisymmetric CH_2 stretching, 1710 cm^{-1} is the C=O stretching, and 1630 cm^{-1} is sometimes assigned to the O–H vibrations due to the presence of adsorbed water [47]. This doublet may correspond to keto–enol tautomerism, an equilibrium known to occur in molecules carrying keto and enol groups. The peak at 1384 cm^{-1} can correspond to the bending vibrations of O–H or C–H. The peak at 1090 cm^{-1} can be related to an alkoxy (R–O) or to the stretching vibration of C–OH in the alcoholic group. The interaction of GO and rAsGFP produces a different spectrum (Fig. 2c) in comparison with pristine GO (Fig. 2a).

Any variation takes place for the O–H stretching frequencies. At the fingerprint region, the relative intensity of keto–enol doublet is modified. The peak at 1710 cm^{-1} is lowered with the presence of rAsGFP, while the peak at 1630 cm^{-1} retains the same position with a shoulder at

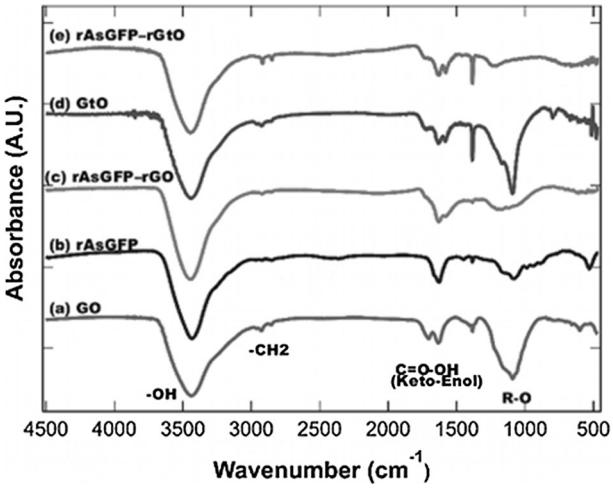

Fig. 2 FTIR spectra for **a** GO, **b** rAsGFP, **c** rAsGFP-rGO, **d** GtO, and **e** rAsGFP-rGtO. Pellets are made using KBr, after drying the material in an oven for 12 h. The main frequencies are detected for OH (3439 cm^{-1}), CH2 (2920 and 2850 cm^{-1}), keto–enol tautomerism (1710 and 1620 cm^{-1}), C=O (1716 cm^{-1} for GtO), OH (1384 cm^{-1}), C–O (1090 cm^{-1})

1583 cm^{-1}. Below 1300 cm^{-1}, only a broad peak is recorded. A possible explanation about the vanishing of the peak at 1090 cm^{-1} (C–O) and the peak at 1710 cm^{-1} can be gathered from the consideration on keto–enol equilibrium. In the GO spectrum, the keto and the enol forms are almost the same, but in the presence of rAsGFP, the protein can interact with the alkoxy (1090 cm^{-1}) reducing and broadening the peak. In consequence, the tautomeric equilibrium may shift toward the enol form, reducing drastically the keto form; hence, the peak at 1710 cm^{-1} almost vanishes. Analogous results are obtained for the reduction of GtO by rAsGFP (Fig. 2e). The peculiar effect is found again for the broadening of the frequencies around 1090 cm^{-1}. An evidence of the GO reduction process was investigated by Zhang et al. [20] and Fernandez-Merino et al. [48]. The authors studied the interaction of GO with L-ascorbic acid reporting the suppression of the R–O frequency similar to our spectra (Fig. 2c, e). The photoluminescent characteristics of the two reduced products, i.e., rAsGFP-rGO and rAsGFP-rGtO, were investigated and compared with the starting materials. In particular, in Fig. 3a, we show the emission spectrum of rAsGFP, GO, and rAsGFP-rGO. Concerning rAsGFP, we observed an intense fluorescence emission band, once excited in the visible range (λ_{ex} 470 nm). It presents a single main peak at 500 nm with a shoulder at about 530 nm. The liquid suspension of GO and GtO exhibited an equivalent PL peak centered at around at 446 nm (λ_{ex} 330 nm). After the reduction with rAsGFP, we analyzed the products of the reaction. It is evident that the reduced sample lost the luminescent characteristics of GO as the typical fluorescence of rAsGFP. Typical PL spectra of a GO suspension cover a broad visible range (from 500 to 800 nm) [49, 50] and the blue region around 390 to 440 nm [51, 52]. Radiative recombination of electron–hole pairs in localized sp^2 domains could give PL effects [45, 53]. In Fig. 3b, we show the emission band of the rAsGFP-rGtO using the two representative excitation wavelengths of GtO and rAsGFP. As a previous plot, we measured the photoluminescent band of GtO (λ_{ex} 330 nm) and fluorescent band of rAsGFP (λ_{ex} 470 nm). The reduced sample behavior was analyzed applying the same excitation parameters. As occurred for rAsGFP-rGO, the rAsGFP-GtO was entirely quenched in its photoluminescent characteristic. Relatively, at the blue [45, 54] and redshift [49] of the GO and rGO fluorescence, many authors have contributed to explain this phenomenon. Maiti et al. [55] focused their attention on the role of different oxygenated functional groups for the tuning of the optical

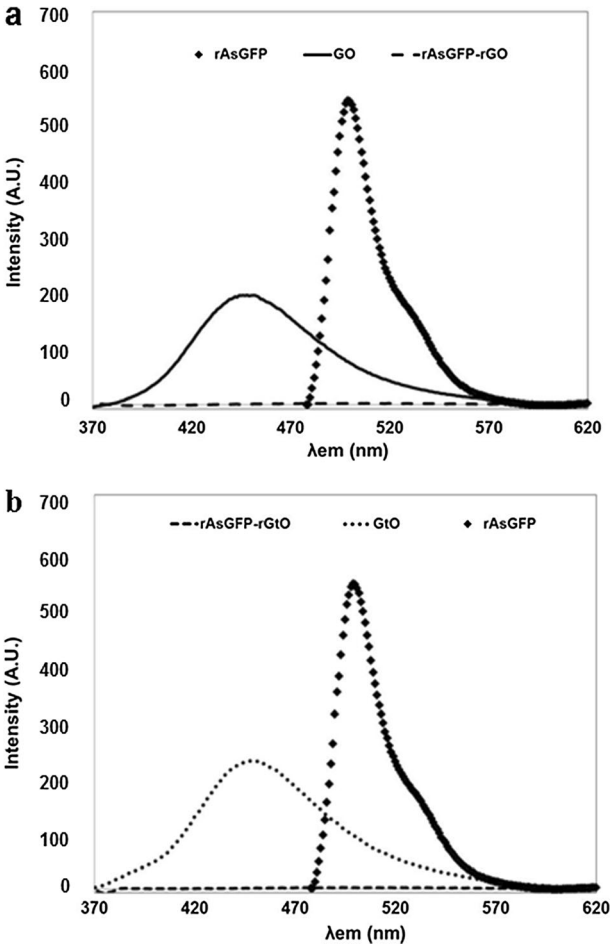

Fig. 3 PL spectra of GO (λ_{ex} 330 nm), rAsGFP-rGO (λ_{ex} 330/470 nm), and rAsGFP (λ_{ex} 470 nm) (**a**), and PL spectra of GtO (λ_{ex} 330 nm), rAsGFP-rGtO (λ_{ex} 330/470 nm), and rAsGFP (λ_{ex} 470 nm) (**b**)

properties of GO defined as the modulation of the sp^2 to sp^3 fraction ratio by the gradual reduction of GO is a way to adapt the optical properties. The partially reduced GO solution after photothermal reduction is a gradual shift of the PL peaks, but for longer exposure, the quenching of the PL signal was evident [45]. Thus, the quenching in our systems can be attributed to a massive reduction of GO and GtO species by means of rAsGFP and a possible effect of shielding of the groups responsible for PL.

In Vitro Hemolytic Activity

The hemolytic activity of GO, GtO, graphite, and GO (Graphenea, 50 % O) is shown in Fig. 4a, where two kinds of trends can be noticed. In particular, the dose/response of GO (Graphenea) shows an increase of hemolysis until a value of concentration of 100 μg mL^{-1} (82 % of hemolysis) followed by a small decrease at 200 μg mL^{-1}, while graphite and GO and GtO synthesized in this work manifest a comparable flat trend. Indeed, in the range of concentrations investigated, we observed a 5 % concentration of cellular lysis for 50 μg mL^{-1} of GO and GtO, while graphite did not show any effects. This can be explained considering the

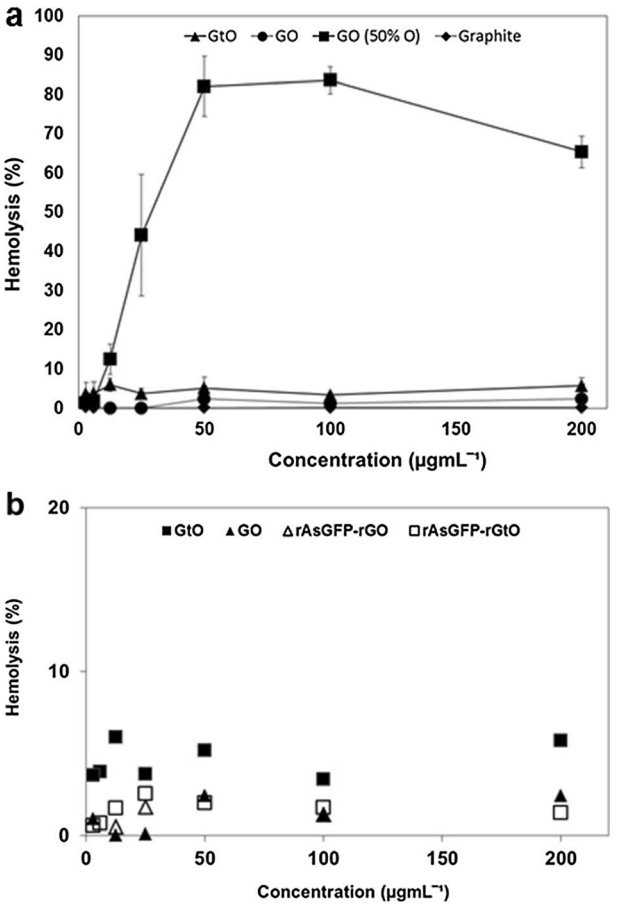

Fig. 4 Trends of erythrocyte hemolysis related to GtO (*triangle*), GO (*circle*), GO (50 % O) (*square*), and graphite (*diamond*) in a range of concentration from 0 to 200 mg mL^{-1} (**a**), and average of the hemolysis values in the entire range of concentration for rAsGFP-rGO and rAsGFP-rGtO compared to GO and GtO (**b**)

relationship between the exfoliation degree and the oxygen content of these materials and their ability of crossing the RBCs membrane. In this regard, Liao and coworkers defined, as the repeated cycles of sonication determined, a higher hemolytic activity probably for the greater extent of exfoliation and smaller size of GO samples [42]. Taking into account this hypothesis, let us consider the exfoliation of our samples. For what regards the commercial compound studied in this work, GO (Graphenea), it has a typical monolayer structure, while the expanded graphite is a powder (40–50 μm). Therefore, the high hemolytic activity of GO (Graphenea) and the low hemolytic activity of expanded graphite can be easily explained in terms of the exfoliation degree, but this cannot be elucidated as observed for GO and GtO. Then, let us consider the oxygen content in our sample, other parameters that seem to be influential for the hemolytic activities [42]. The carbon/oxygen (C/O) ratio of graphene oxide species is strongly related to the methodologies employed for the synthesis. In particular, the Hummers method [56] allows us to obtain species with C/O values between 1.8 and 2.5, while the Sun method [57] leads to a less oxidized species with a C/O ratio value of about 3. The similar carbon and oxygen atoms ratio in GO (22 % O) and GtO (24 % O) explained the same trend of RBCs lysis despite the different degrees of exfoliation. For GO (Graphenea, 50 % O), the hemolysis was

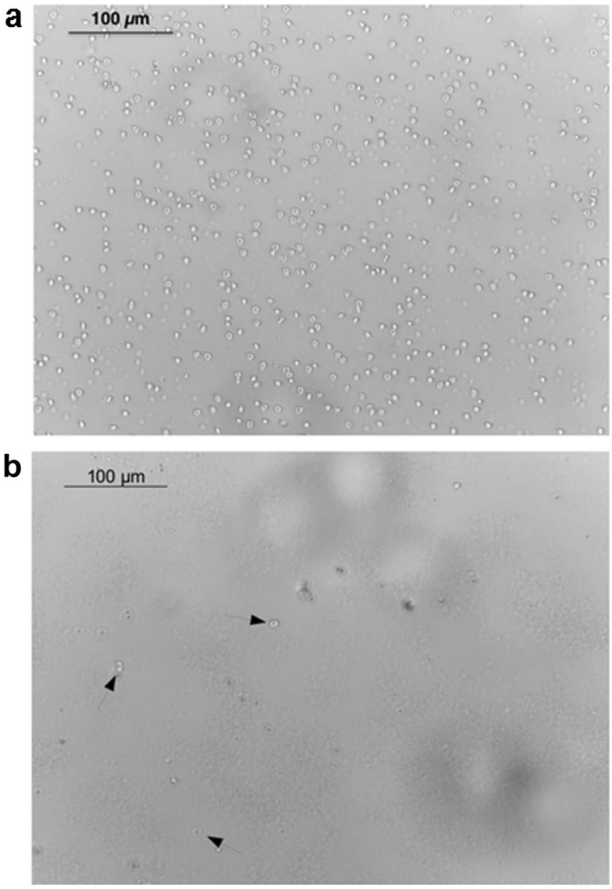

Fig. 5 RBCs suspensions of negative control (**a**) and GO (Graphenea) at 200 mg mL^{-1} (**b**) after the incubation of samples

the result of two coupled parameters, the exfoliation and the higher presence of oxygen atoms, respectively. These results suggest that the hemolysis is caused by the strong interaction between polarized groups -CO, -OCO- of graphene and graphite oxide and the polar head of phosphatidylcholine on the RBCs' membrane.

To value if the reduced species with the rAsGFP can be used as a biocompatible vehicle, we tested the hemolytic activity of rAsGFP-rGO and rAsGFP-rGtO on the RCBs. In Fig. 4b, we show the behavior of reduced graphene and graphite oxide species and their respective initial compounds. In the range of the investigated concentration, no differences in the trend of each species were observed. Moreover, making an average of the hemolysis values in the entire range of concentration for rAsGFP-rGtO, we measured a decrease with respect to the erythrocyte lysis compared to GtO. Their differences were less evident in the case of rAsGFP-rGO and GO compounds. This is indicative of a good biocompatibility of our initial synthesis compounds. The erythrocyte lysis was evident after the observation of RCBs treated with GO (Graphenea) by optical microscopy. Figure 5b shows the strong decrease in the RBCs' density following the treatment and incubation with 200 μg mL^{-1} of graphene oxide. The negative control in the same condition of incubation is shown in Fig. 5a.

Conclusions

We analyzed the RBCs' biocompatibility of GO and GtO and their reduced species, focusing on the exfoliation degree and the oxygen content of many samples which are known to have a critical role in extent of hemolysis. The results of hemolytic assays suggested that since their RBCs biocompatibility, these materials can be used to carry drugs in circle. In particular, in our synthetic strategies, we are able to obtain a single layer for GO and a multilayer for GtO with a similar carbon and oxygen atom ratio. They revealed a comparable trend and a negligible effect on the RBCs' lysis. Indeed, the synthesis of GO and GtO by means of a temperature-controlled modified Sun protocol lead to a biocompatible species with a lower oxygen content species than the commercial compound studied in this work. Compared to dispersed GO and GtO sheets, the reduced samples showed a lower hemolytic activity. Thus, the low-cost and fast synthesis of rAsGFP-rGO and rAsGFP-rGtO with the green fluorescent protein as reducing and stabilizing agent allowed us to obtain smart biocompatible and environmentally friendly materials. In fact, this approach does not require hazardous and toxic reagents. Furthermore, the controlled release of rAsGFP could represent a promising method for in vivo imaging of pharmaceutical preparation introduced by means of intravenous administration. With this purpose, further studies are in progress to evaluate the reversibility of the reaction of GO and GtO with the rAsGFP.

Acknowledgments This work was supported by PON Ricerca e Competitività 2007/2013, PON FILM-EDIBILI "(Cod. PON01 02286), Progetto Strategico MAESTRA" funded by the University of Padova.

References

1. Novoselov, K. S., Geim, A. K., Morozov, S. V., Jiang, D., Zhang, Y., Dubonos, S. V., Grigorieva, I. V., & Firsov, A. A. (2004). Electric field effect in atomically thin carbon films. *Science, 306*, 666–669.
2. Tung, V. C., Allen, M. J., Yang, Y., & Kaner, R. B. (2008). High-throughput solution processing of large-scale graphene. *Nature Nanotechnology, 4*, 25–29.
3. Allen, M. J., Tung, V. C., Kaner R. B. (2010). Honeycomb carbon: a review of graphene. *Chemical Reviews, 110*, 132–145.
4. Emtsev, K. V., Bostwick, A., Horn, K., Jobst, J., Kellogg, G. L., Ley, L., McChesney, J. L., Ohta, T., Reshanov, S. A., Röhrl, J., Rotenberg, E., Schmid, A. K., Waldmann, D., Weber, H. B., & Seyller, T. (2009). Towards wafer-size graphene layers by atmospheric pressure graphitization of silicon carbide. *Nature Materials, 8*, 203–207.
5. Zhou, S. Y., Siegel, D. A., Fedorov, A. V., Gabaly, F. E., Schmid, A. K., Neto, A. H. C., Lee, D. H., & Lanzara, A. (2008). Origin of the energy bandgap in epitaxial graphene. *Nature Materials, 7*, 259–260.
6. Higginbotham, A. L., Kosynkin, D. V., Sinitskii, A., Sun, Z., & Tour, J. M. (2010). Lower-defect graphene oxide nanoribbons from multiwalled carbon nanotubes. *ACS Nano, 4*, 2059–2069.
7. Chua, C. K., & Pumera, M. (2014). Chemical reduction of graphene oxide: a synthetic chemistry viewpoint. *Chemical Society Reviews, 43*, 291–312.
8. Xu, J., Wang, K., Zu, S. Z., Han, B. H., & Wei, Z. (2010). Hierarchical nanocomposites of polyaniline nanowire arrays on graphene oxide sheets with synergistic effect for energy storage. *ACS Nano, 4*, 5019–5026.
9. Cote, L. J., Kim, J., Tung, V. C., Luo, J., Kim, F., & Huang, J. (2011). Graphene oxide as surfactant sheets. *Pure and Applied Chemistry, 83*, 95–110.
10. Kemp, K. C., Seema, H., Saleh, M., Le, N. H., Mahesh, K., Chandra, V., & Kim, K. S. (2013). Environmental applications using graphene composites: water remediation and gas adsorption. *Nanoscale, 5*, 3149.

11. Liu, Y., Yu, D., Zeng, C., Miao, Z., & Dai, L. (2010). Biocompatible graphene oxide-based glucose biosensors. *Langmuir, 26*, 6158–6160.
12. Becerril, H. A., Stoltenberg, R. M., Tang, M. L., Roberts, M. E., Liu, Z., Chen, Y., Kim, D. H., Lee, B.-L., Lee, S., & Bao, Z. (2010). Fabrication and evaluation of solution processed reduced graphene oxide electrodes for P- and N-channel bottom-contact organic thin-film transistors. *ACS Nano, 4*, 6343–6352.
13. Bagri, A., Mattevi, C., Acik, M., Chabal, Y. J., Chhowalla, M., & Shenoy, V. B. (2010). Structural evolution during the reduction of chemically derived graphene oxide. *Nature Chemistry, 2*, 581–587.
14. Shin, H.-J., Kim, K. K., Benayad, A., Yoon, S.-M., Park, H. K., Jung, I.-S., Jin, M. H., Jeong, H.-K., Kim, J. M., Choi, J.-Y., & Lee, Y. H. (2009). Efficient reduction of graphite oxide by sodium borohydride and its effect on electrical conductance. *Advanced Functional Materials, 19*, 1987–1992.
15. Botas, C., Alvarez, P., Blanco, C., Gutierrez, M. D., Ares, P., Zamani, R., Arbiol, J., Morante, J. R., & Menendez, R. (2012). Tailored graphene materials by chemical reduction of graphene oxides of different atomic structure. *RSC Advances, 2*, 9643–9650.
16. Patil, A. J., Vickery, J. L., Scott, T. B., & Mann, S. (2009). Aqueous stabilization and self-assembly of graphene sheets into layered bio-nanocomposites using DNA. *Advanced Materials, 21*, 3159–3164.
17. Grayfer, E. D., Makotchenko, V. G., Nazarov, A. S., Kim, S. J., & Fedorov, V. E. (2011). Graphene: chemical approaches to the synthesis and modification. *Russian Chemical Reviews, 80*, 751–770.
18. Eigler, S., Grimm, S., Enzelberger-Heim, M., Müller, P., & Hirsch, A. (2013). Graphene oxide: efficiency of reducing agents. *Chemical Communications, 49*, 7391–7393.
19. Ambrosi, A., Chua, C. K., Bonanni, A., & Pumera, M. (2012). Lithium aluminum hydride as reducing agent for chemically reduced graphene oxides. *Chemistry of Materials, 24*, 2292–2298.
20. Zhang, J., Yang, H., Shen, G., Cheng, P., Zhang, J., & Guo, S. (2010). Reduction of graphene oxide vial-ascorbic acid. *Chemical Communications, 46*, 1112.
21. Kotchey, G. P., Allen, B. L., Vedala, H., Yanamala, N., Kapralov, A. A., Tyurina, Y. Y., Klein-Seetharaman, J., Kagan, V. E., & Star, A. (2011). The enzymatic oxidation of graphene oxide. *ACS Nano, 5*, 2098–2108.
22. Georgakilas, V., Otyepka, M., Bourlinos, A. B., Chandra, V., Kim, N., Kemp, K. C., Hobza, P., Zboril, R., & Kim, K. S. (2012). Functionalization of graphene: covalent and non-covalent approaches, derivatives and applications. *Chemical Reviews, 112*, 6156–6214.
23. Su, C., & Loh, K. P. (2012). Carbocatalysts: graphene oxide and its derivatives. *Accounts of Chemical Research, 46*, 2275–2285.
24. Gurunathan, S., Han, J. W., Kim, E., Kwon, D.-N., Park, J.-K., & Kim, J.-H. (2014). Enhanced green fluorescent protein-mediated synthesis of biocompatible graphene. *Journal of Nanbiotechnology, 12*, 41.
25. Heim, R., Prasher, D. C., & Tsien, R. Y. (1994). Wavelength mutations and post translational autoxidation of green fluorescent protein. *Proceedings of the National Academy of Sciences of the United States of America, 91*, 12501–12504.
26. Rafat, M., Cleroux, C. A., Fong, W. G., Baker, A. N., Leonard, B. C., O'Connor, M. D., & Tsilfidis, C. (2010). PEG-PLA microparticles for encapsulation and delivery of TAT-EGFP to retinal cells. *Biomaterials, 31*, 3414–3421.
27. Brocklehurst, K., & Little, G. (1972). Reactivities of the various protonic states in the reactions of papain and of L-cysteine with 2, 2′-and with 4, 4′-dipyridyl disulphide: evidence for nucleophilic reactivity in the un-ionized thiol group of the cysteine-25 residue of papain occasioned by its interaction with the histidine-159-asparagine-175 hydrogen-bonded system. *Biochemical Journal, 128*, 471.
28. Hu, W., Peng, C., Luo, W., Lv, M., Li, X., Li, D., Huang, Q., & Fan, C. (2010). Graphene-based antibacterial paper. *ACS Nano, 4*, 4317–4323.
29. Sun, X., Liu, Z., Welsher, K., Robinson, J. T., Goodwin, A., Zaric, S., & Dai, H. (2008). Nano-graphene oxide for cellular imaging and drug delivery. *Nano Research, 1*, 203–212.
30. Yang, K., Zhang, S., Zhang, G., Sun, X., Lee, S.-T., & Liu, Z. (2010). Graphene in mice: ultrahigh in vivo tumor uptake and efficient photothermal therapy. *Nano Letters, 10*, 3318–3323.
31. Akhavan, O., & Ghaderi, E. (2010). Toxicity of graphene and graphene oxide nanowalls against bacteria. *ACS Nano, 4*, 5731–5736.
32. Cheng, L.-C., Jiang, X., Wang, J., Chen, C., & Liu, R.-S. (2013). Nano-bio effects: interaction of nanomaterials with cells. *Nanoscale, 5*, 3547–3569.
33. Wang, K., Ruan, J., Song, H., Zhang, J., Wo, Y., Guo, S., & Cui, D. (2011). Biocompatibility of graphene oxide. *Nanoscale Research Letters, 6*, 1–8.
34. Sanchez, V. C., Jachak, A., Hurt, R. H., & Kane, A. B. (2011). Biological interactions of graphene-family nanomaterials: an interdisciplinary review. *Chemical Research in Toxicology, 25*, 15–34.
35. Lu, C.-H., Yang, H.-H., Zhu, C.-L., Chen, X., & Chen, G.-N. (2009). A graphene platform for sensing biomolecules. *Angewandte Chemie, 121*, 4879–4881.

36. Nayak, T. R., Andersen, H., Makam, V. S., Khaw, C., Bae, S., Xu, X., Ee, P.-L. R., Ahn, J.-H., Hong, B. H., Pastorin, G., & Ozyilmaz, B. (2011). Graphene for controlled and accelerated osteogenic differentiation of human mesenchymal stem cells. *ACS Nano, 5*, 4670–4678.
37. Song, Y., Qu, K., Zhao, C., Ren, J., & Qu, X. (2010). Graphene oxide: intrinsic peroxidase catalytic activity and its application to glucose detection. *Advanced Materials, 22*, 2206–2210.
38. Tsien, R. Y. (1998). The green fluorescent protein. *Annual Review of Biochemistry, 67*, 509–544.
39. Chudakov, D. M., Belousov, V. V., Zaraisky, A. G., Novoselov, V. V., Staroverov, D. B., Zorov, D. B., Lukyanov, S., & Lukyanov, K. A. (2003). Kindling fluorescent proteins for precise in vivo photolabeling. *Nature Biotechnology, 21*, 191–194.
40. Masullo, T., Puccio, R., Di Pierro, M., Tagliavia, M., Censi, P., Vetri, V., Militello, V., Cuttitta, A., & Colombo, P. (2014). Development of a biosensor for copper detection in aqueous solutions using an anemonia sulcata recombinant GFP. *Applied Biochemistry and Biotechnology, 172*, 2175–2187.
41. Pendolino, F., Capurso, G., Maddalena, A., & Lo Russo, S. (2014). The structural change of graphene oxide in a methanol dispersion. *RSC Advances, 4*, 32914–32917.
42. Liao, K.-H., Lin, Y.-S., Macosko, C. W., & Haynes, C. L. (2011). Cytotoxicity of graphene oxide and graphene in human erythrocytes and skin fibroblasts. *ACS Applied Materials & Interfaces, 3*, 2607–2615.
43. Lai, Q., Zhu, S., Luo, X., Zou, M., & Huang, S. (2012). Ultraviolet-visible spectroscopy of graphene oxides. *AIP Advances, 2012*(2), 032146.
44. Chien, C. T., Li, S. S., Lai, W. J., Yeh, Y. C., Chen, H. A., Chen, I. S., Chen, L. C., Chen, K. H., Nemoto, T., Isoda, S., Chen, M., Fujita, T., Eda, G., Yamaguchi, H., Chhowalla, M., Chen, C. W. (2012). Tunable photoluminescence from graphene oxide. *Angewandte Chemie International Edition, 51*, 6662–6666.
45. Eda, G., Lin, Y.-Y., Mattevi, C., Yamaguchi, H., Chen, H.-A., Chen, I., Chen, C.-W., & Chhowalla, M. (2010). Blue photoluminescence from chemically derived graphene oxide. *Advanced Materials, 22*, 505–509.
46. Pendolino, F., Parisini, E., & Lo Russo, S. (2014). Time-dependent structure and solubilization kinetics of graphene oxide in methanol and water dispersions. *Journal of Physical Chemistry C, 118*, 28162–28169.
47. Kaniyoor, A., Baby, T. T., & Ramaprabhu, S. (2010). Graphene synthesis via hydrogen induced low temperature exfoliation of graphite oxide. *Journal of Materials Chemistry, 20*, 8467–8469.
48. Fernandez-Merino, M. J., Guardia, L., Paredes, J. I., Villar-Rodil, S., Solis-Fernandez, P., Martinez-Alonso, A., & Tascon, J. M. D. (2010). Vitamin C is an ideal substitute for hydrazine in the reduction of graphene oxide suspensions. *Journal of Physical Chemistry C, 114*, 6426–6432.
49. Luo, Z., Vora, P. M., Mele, E. J., Johnson, A. C., & Kikkawa, J. M. (2009). Photoluminescence and band gap modulation in graphene oxide. *Applied Physics Letters, 94*, 111909.
50. Maiti, R., Manna, S., Midya, A., & Ray, S. K. (2013). Broadband photoresponse and rectification of novel graphene oxide/n-Si heterojunctions. *Optics Express, 21*, 26034–26043.
51. Xin, G., Meng, Y., Ma, Y., Ho, D., Kim, N., Cho, S. M., & Chae, H. (2012). Tunable photoluminescence of graphene oxide from near-ultraviolet to blue. *Materials Letters, 74*, 71–73.
52. Pan, D., Zhang, J., Li, Z., & Wu, M. (2010). Hydrothermal route for cutting graphene sheets into blue-luminescent graphene quantum dots. *Advanced Materials, 22*, 734–738.
53. Mei, Q., Zhang, K., Guan, G., Liu, B., Wang, S., & Zhang, Z. (2010). Highly efficient photoluminescent graphene oxide with tunable surface properties. *Chemical Communications, 46*, 7319–7321.
54. Shang, J., Ma, L., Li, J., Ai, W., Yu, T., Gurzadyan, G. G. (2012). The origin of fluorescence from graphene oxide. *Scientific Reports 2*, 792. doi:10.1038/srep00792.
55. Maiti, R., Midya, A., Narayana, C., & Ray, S. (2014). Tunable optical properties of graphene oxide by tailoring the oxygen functionalities using infrared irradiation. *Nanotechnology, 25*, 495704.
56. Hummers, W. S., & Offeman, R. E. (1958). Preparation of graphitic oxide. *Journal of the American Chemical Society, 80*, 1339.
57. Sun, L., & Fugetsu, B. (2013). Mass production of graphene oxide from expanded graphite. *Materials Letters, 109*, 207–210.